

HIGH-ENERGY HADRON SPIN-FLIP AMPLITUDE¹

*O.V. Selyugin*²

Joint Institute for Nuclear Research, Dubna

The high-energy part of the hadron spin-flip amplitude is examined in the framework of the new high-energy general structure (HEGS) model of the elastic hadron scattering at high energies. The different forms of the hadron spin-flip amplitude are compared in the impact parameter representation. It is shown that the existing experimental data of the proton–proton and proton–antiproton elastic scattering at high energy in the region of the diffraction minimum and at large momentum transfer give support in the presence of the energy-independent part of the hadron spin-flip amplitude with the momentum dependence proposed in the works by Galynskii–Kuraev.

На основе новой, с учетом обобщенной структуры, высокоэнергетической модели упругого рассеяния нуклонов исследована высокоэнергетическая часть адронной спин-флиповой амплитуды рассеяния. Различные виды адронной спин-флиповой амплитуды вычисляются и сравниваются в представлении прицельного параметра. Показано, что существующие экспериментальные данные по протон-протонному и протон-антипротонному упругому рассеянию при высоких энергиях и в области дифракционного минимума, и при больших моментах передачи импульса подтверждают присутствие энергетически независимой части адронной спин-флиповой амплитуды с кинематическим фактором, предложенным в работах Галынского–Кураева.

PACS: 11.80-m; 11.80.Cr; 13.75.Cs; 13.85.Dz

INTRODUCTION

The spin effects very often play the touchstone role for many different theoretical approaches. Especially, it applies to the hadron–hadron elastic processes. The famous experiments carried out by A. Krish at the ZGS to obtain the spin-dependent differential cross sections [1, 2] and the spin-correlation parameter A_{NN} [3] and at the AGS [4] to obtain the spin-correlation parameter A_N showed the significant spin effects at large momentum transfer. Note that the spin-flip amplitudes, determined by the nonleading Reggions exchange, give a large contribution only at small momentum transfer, as the massive nonleading Reggions have a large slope and decrease faster at large t . Of course, many questions arise about the energy dependence of the spin-flip amplitudes and the relative phase between the spin-nonflip and spin-flip amplitudes. Now there are many different models for the description of the elastic hadron scattering amplitude [5, 6]. They lead to different predictions of the structure

¹Talk at the Workshop “Selected Problems in Quantum Field Theory”, Dubna (2015), dedicated to the memory of Prof. E. A. Kuraev.

²E-mail: selugin@theor.jinr.ru

of the scattering amplitude at high energies. The diffraction processes at very high energies, especially in the TeV energy region, are simplified by the asymptotical regime but can display complicated features [7, 8].

According to the standard opinion, the hadron spin-flip amplitude is connected with the quark exchange between the scattering hadrons, and at large energy it can be neglected. Some models, which take into account the nonperturbative effects, lead to the nondying hadron spin-flip amplitude [9–13]. Another complicated question is related to the difference in phases of the spin-nonflip and spin-flip amplitudes.

The description of the high-energy processes requires using some unitarization procedures of the Born scattering amplitude. They are related to the different forms of the summation of some sets of diagrams of the tree approximation. The unitarization leads to the asymptotic unitarity bound connected with the so-called Black Disk Limit (BDL), which can lead to different saturation effects [14]. In the partial wave language, we need to sum many different waves with $l \rightarrow \infty$, and this leads to the impact parameter representation [15] converting the summation over l into integration over b .

1. SPIN-DEPENDENT SCATTERING AMPLITUDE

In the Regge limit t_{fix} and $s \rightarrow \infty$ one can write the Regge-pole contributions to the helicity amplitudes in the s -channel as [16]

$$\Phi_{\lambda_1, \lambda_2, \lambda_3, \lambda_4}^B(s, t) \sim \sum_i g_{\lambda_1, \lambda_2}^i(t) g_{\lambda_3, \lambda_4}^i(t) [\sqrt{|t|}]^{|\lambda_1 - \lambda_2| + |\lambda_3 - \lambda_4|} \left(\frac{s}{s_0}\right)^{\alpha_i} (1 \pm e^{-i\pi\alpha_i}). \quad (1)$$

A convenient basis in terms of helicities, where the corresponding amplitudes of proton–proton scattering are in the s -channel [17], is

$$\begin{aligned} \Phi_1^B(s, t) &= \langle ++ | ++ \rangle, & \Phi_2^B(s, t) &= \langle ++ | -- \rangle, & \Phi_3^B(s, t) &= \langle +- | +- \rangle, \\ \Phi_4^B(s, t) &= \langle +- | -+ \rangle, & \Phi_5^B(s, t) &= \langle ++ | +- \rangle. \end{aligned} \quad (2)$$

The differential cross section is

$$\frac{d\sigma}{dt} = \frac{2\pi}{s^2} (|\Phi_1|^2 + |\Phi_2|^2 + |\Phi_3|^2 + |\Phi_4|^2 + 4|\Phi_5|^2). \quad (3)$$

The total helicity amplitudes can be written as

$$\Phi_i(s, t) = \Phi_i^h(s, t) + \Phi_i^{\text{em}}(s, t) e^{\varphi(s, t)}, \quad (4)$$

where $\Phi_i^h(s, t)$ is the pure strong interaction of hadrons; $\Phi_i^{\text{em}}(s, t)$ is the electromagnetic interaction of hadrons, and $\varphi(s, t)$ is the electromagnetic-hadron interference phase factor [18, 19]. The corresponding spin-correlation values will be

$$A_N \frac{d\sigma}{dt} = -\frac{4\pi}{s^2} [\text{Im}(\Phi_1(s, t) + \Phi_2(s, t) + \Phi_3(s, t) - \Phi_4(s, t)) \Phi_5^*(s, t)] \quad (5)$$

and

$$A_{NN} \frac{d\sigma}{dt} = \frac{4\pi}{s^2} [\text{Re}(\Phi_1(s, t) \Phi_2^*(s, t) - \Phi_3(s, t) \Phi_4^*(s, t)) + |\Phi_5(s, t)|^2]. \quad (6)$$

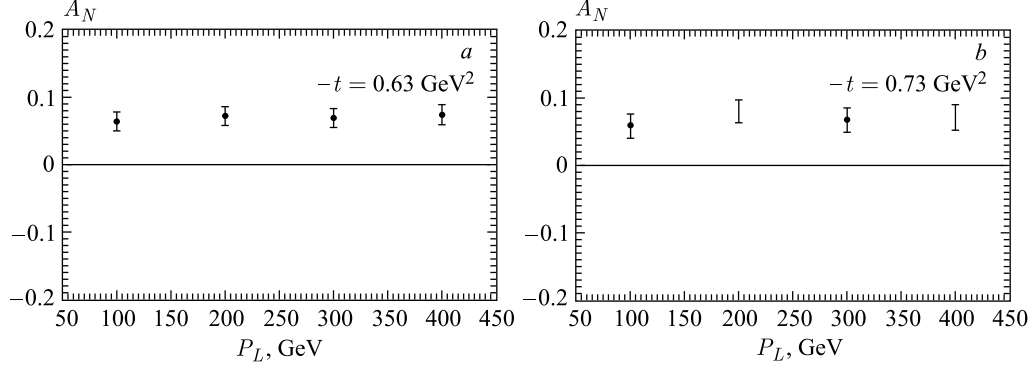


Fig. 1. Energy dependence of the experimental data of the spin-correlation parameter $A_N(s, t)$ at some separate point of the momentum transfer [21] at $-t = 0.63 \text{ GeV}^2$ (a) and at $-t = 0.73 \text{ GeV}^2$ (b)

The s -channel factorization together with the experimental information about the spin-correlation effects at high energy and small momentum transfer in the proton–proton elastic scattering suggests that the double helicity flip is a second-order effect and, consequently, the amplitudes $\Phi_{+--+}^B(s, t)$ and $\Phi_{+---}^B(s, t)$ can be neglected. Furthermore, when the exchange of Regge poles has natural parity, we have for the spin-nonflip amplitudes [20] $\Phi_{++++}^B(s, t) = \Phi_{+--+}^B(s, t)$.

Neglecting the $\Phi_2(s, t) - \Phi_4(s, t)$ contribution, the spin-correlation parameter $A_N(s, t)$ can be written taking into account the phases of separate amplitudes

$$A_N(s, t) \frac{d\sigma}{dt} = -\frac{4\pi}{s^2} [|F_{\text{nf}}(s, t)| |F_{\text{sf}}(s, t)|] \sin(\phi_{\text{nf}}(s, t) - \phi_{\text{sf}}(s, t)), \quad (7)$$

where $\phi_{\text{nf}}(s, t)$, $\phi_{\text{sf}}(s, t)$ are the phases of the spin-nonflip and spin-flip amplitudes. It is clearly seen that despite the large spin-flip amplitude the analyzing power can be near zero if the difference of the phases is zero in some region of momentum transfer. The experimental data at some point of the momentum transfer show the energy independence of the size of the spin-correlation parameter $A_N(s, t)$ (see Fig. 1). Hence, the small value of the $A_N(s, t)$ at some t (for example, very small t) does not serve as a proof that it will be small in other regions of momentum transfer.

2. ELASTIC NUCLEON SCATTERING (HEGS MODEL)

In some early models of the elastic hadron scattering the hadron was regarded as the whole particle and the diffraction occurred on the surface [22,23] of the hadron. The parton structure of the hadron can be related to the hadron form factors and the elastic scattering amplitude is proportional to these form factors [24]. Some models take into account the parton structure of the hadron as separate interactions of the gluons and quarks [25]. A more complicated picture of the hadron structure appears with introducing the nonforward parton structure — general parton distributions (GPDs) and transfer momentum distributions (TMDs). The different moments of GPDs allow us to calculate the different hadron form factors, such as Compton

form factors ($R_V(t)$, $R_T(t)$, $R_A(t)$), electromagnetic form factors ($F_1(t)$, $F_2(t)$), and the so-called gravimagnetic form factors ($A(t)$, $B(t)$) [26–28].

Let us use the obtained momentum transfer dependence of GPDs to calculate the electromagnetic and gravimagnetic form factors of the nucleons as the first and second moments of GPDs [29, 30]. The obtained form factors are related to the charge and matter distributions. By fixing the parameters of the obtained form factors the new high-energy general structure (HEGS) model of the elastic proton–proton and proton–antiproton scattering was proposed [31, 32].

The HEGS model [32] gives a quantitative description of the elastic nucleon scattering at high energy with only five fitting high-energy parameters. A successful description of the existing experimental data by the model shows that the elastic scattering is determined by the generalized structure of the hadron. The model leads to a coincidence of the model calculations with the preliminary data at 8 TeV. We found that the standard eikonal approximation [33] works perfectly well from $\sqrt{s} = 9$ GeV up to $\sqrt{s} = 8$ TeV.

In the model, the Born term of the elastic hadron amplitude is determined as

$$F_h^{\text{Born}}(s, t) = h_1 F_1^2(t) F_a(s, t) \left(1 + \frac{r_1}{\hat{s}^{0.5}}\right) + h_2 A^2(t) F_b(s, t) \left(1 + \frac{r_2}{\hat{s}^{0.5}}\right), \quad (8)$$

where $F_a(s, t)$ and $F_b(s, t)$ have the standard Regge form:

$$F_a(s, t) = \hat{s}^{\epsilon_1} e^{B(s)t}, \quad F_b(s, t) = \hat{s}^{\epsilon_1} e^{B(s)/4t}. \quad (9)$$

The form factors $F_1(t)$ and $A(t)$ are determined by the first and second moments of GPDs, respectively, and reflect the charge and matter distributions.

The model takes into account the odderon contribution with factor $h_{\text{odd}} = ih_3 t / (1 - r_0^2 t)$. So the full Born term of the scattering amplitude is

$$F_h^{\text{Born}}(s, t) = h_1 F_1^2(t) F_a(s, t) \left(1 + \frac{r_1}{\sqrt{\hat{s}}}\right) + h_2 A^2(t) F_b(s, t) \pm h_{\text{odd}} A^2(t) F_b(s, t) \left(1 + \frac{r_2}{\sqrt{\hat{s}}}\right). \quad (10)$$

The terms proportional to $r_1/\sqrt{\hat{s}}$ and $r_2/\sqrt{\hat{s}}$ take into account some possible nonasymptotic contributions.

The size, energy, and momentum transfer dependence of the real part of the elastic scattering amplitude are determined by the complex energy $\hat{s} = s \exp(-i\pi/2)$. Hence, the model does not introduce any special functions or assumptions for the real part of the scattering amplitude. Note that the role of the real part is especially important at low momentum transfer (where the differential cross sections are determined by the Coulomb-hadron interference effects) and in the region of the diffraction minimum (where the imaginary part of the scattering amplitude has the zero, and the size of the diffraction minimum is determined by the real part of the scattering amplitude and the contribution of the spin-flip part of the scattering amplitude).

The hard pomeron contribution was analyzed in the framework of the model [34]. It was shown that such a contribution is very small in the elastic hadron scattering and is not felt in the fitting procedure.

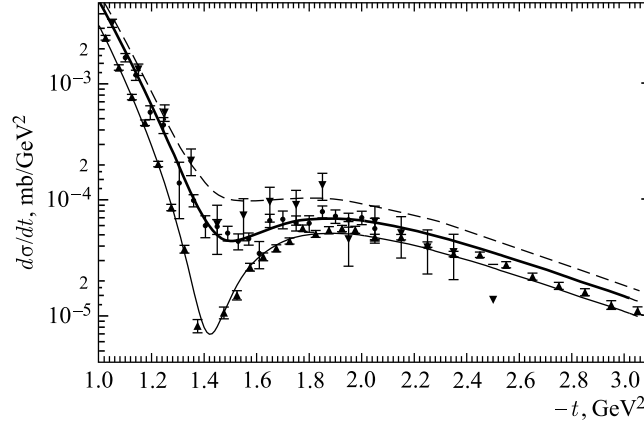


Fig. 2. The energy dependence of the diffraction minimum. The model calculations: dashed line — $\sqrt{s} = 9.78$ GeV; thick solid line — $\sqrt{s} = 19.4$ GeV; thin solid line — $\sqrt{s} = 30.5$ GeV; triangles down, circles, and triangles up — the experimental data at the same energies, respectively

The final elastic hadron scattering amplitude is obtained after unitarization of the Born term. So, first, we have to calculate the eikonal phase. In the most favorable eikonal unitarization scheme the eikonal phase corresponds to the Born term of the scattering amplitude, Eq. (1), and in the common case corresponds to the spin-dependent potential.

The model description of the differential cross sections in such a huge energy region is reflected brightly in the description of the region of the diffraction minimum (see Fig. 2). In most part, the form and energy dependence of the diffraction region is determined by the real part of the scattering amplitude and possible contributions of the spin-flip amplitude. Note that in the HEGS model only the Born term is determined and the complicated diffractive structure is obtained only after the unitarization procedure.

3. IMPACT OF THE SPIN-FLIP CONTRIBUTION

Usually, one makes the assumptions that the imaginary and real parts of the spin-nonflip amplitude have the exponential behavior with the same slope, and the imaginary and real parts of the spin-flip amplitudes, without the kinematic factor $\sqrt{|t|}$ [35], are proportional to the corresponding parts of the nonflip amplitude. For example, in [36] the spin-flip amplitude was chosen in the form

$$F_h^{\text{fl}} = \sqrt{-t}/m_p h_{\text{sf}} F_h^{\text{mf}}. \quad (11)$$

That is not so as regards the t dependence shown in [37], where F_h^{fl} is multiplied by the special function dependent on t . Moreover, one mostly takes the energy independence of the ratio of the spin-flip parts to the spin-nonflip parts of the scattering amplitude. All this is our theoretical uncertainty [38–40].

In [41], on the basis of generalization of the constituent-counting rules of the perturbative QCD, the proton current matrix elements $J_p^{\pm\delta\delta}$ for the full set of spin combinations corresponding to the number of the spin-flipped quarks were calculated. It leads to the part of the

spin-flip amplitude

$$F_h^{sl} \sim \frac{\sqrt{-t}}{(4/9)m_p^2} \frac{\sqrt{-t}}{(4/9)m_p^2} \frac{\sqrt{-t}}{(4/9)m_p^2}. \quad (12)$$

Hence, such an amplitude will give large contributions at large momentum transfer. In the HEGS model the calculations are extended up to $-t = 15 \text{ GeV}^2$, and we added the small contribution of the asymptotically independent energy part of the spin-flip amplitude with the kinematical factor, Eq. (12). So, the form of the spin-flip amplitude is determined as

$$F_{sf}(s, t) = h_{sf} q^3 F_1^2(t) e^{-B_{sf} q^2}. \quad (13)$$

Of course, at lower energy we need to take into account the energy-dependent parts of the spin-flip amplitudes. However, it requires including in our examination additional polarization data and the contributions of the nonleading Reggions, which essentially complicate the picture. Now it is beyond the scope of this paper. Such a contribution can be made in future works.

It is interesting that the spin-flip amplitude in the form (13) can be compared with the spin-flip amplitude with the standard kinematical factor $\sqrt{|t|}$ but with the Gaussian form of the slope

$$F_{sf}(s, t) = h_{sf} q F_1^2(t) e^{-(r-q)^2}. \quad (14)$$

Let us compare the spin-flip amplitudes (13) and (14) in the impact parameter representation

$$F_{sf}(b, t) = \int_0^\infty q dq J_1(q, b) F_{sf}(s, q). \quad (15)$$

The spin-flip amplitudes with the standard kinematical factor, Eq. (13), and with the kinematical factor, Eq. (12), are compared with the spin-flip amplitude, Eq. (14), in Fig. 3, *a*. It can be seen that the standard spin-flip amplitude has more peripheral interactions.

A more obvious result can be obtained by comparing these amplitudes multiplied by the impact parameter b and with the same sizes (we divide the standard amplitude by a factor of 2 and multiply amplitude, Eq. (14), by the same factor). The results are shown in Fig. 3, *b*. The impact dependence of the amplitudes, Eqs. (13) and (14), has a small difference. However,

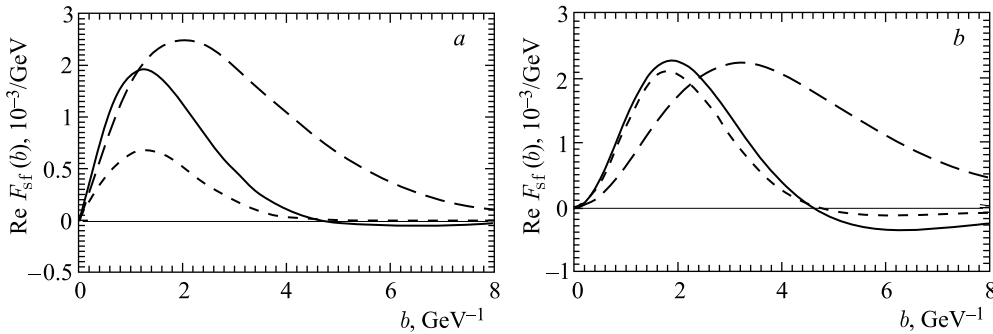


Fig. 3. The spin-flip amplitude in the impact parameter representation (solid line — Eq. (13), dashed line — Eq. (14), long-dashed line — Eq. (13) with the standard kinematical factor q)

the impact dependence of the standard spin-flip amplitude with the kinematical factor $\sqrt{|t|}$ has an essentially different form. It has a more peripheral origin.

As we have already noted, the size of the spin-flip contributions is bounded by the size of the differential cross sections at their diffraction minimum. In Fig. 2, the model calculations are compared for the energy where the diffraction dip has the minimum value. A similar situation for the proton–proton cross sections occurs at $\sqrt{s} = 30$ GeV where the real part changes its sign at $t = 0$. The model calculations describe the form of the diffraction minimum at this energy very well. Moreover, the model sufficiently well reproduces the energy dependence of the differential cross section in the region of the diffraction dip. Note that in the HEGS model the real part of the elastic scattering amplitude is determined by the complex \hat{s} only. So, Fig. 2 shows that the contribution of the spin-flip amplitude is essentially small in this region of the momentum transfer. However, the contributions of the taken form

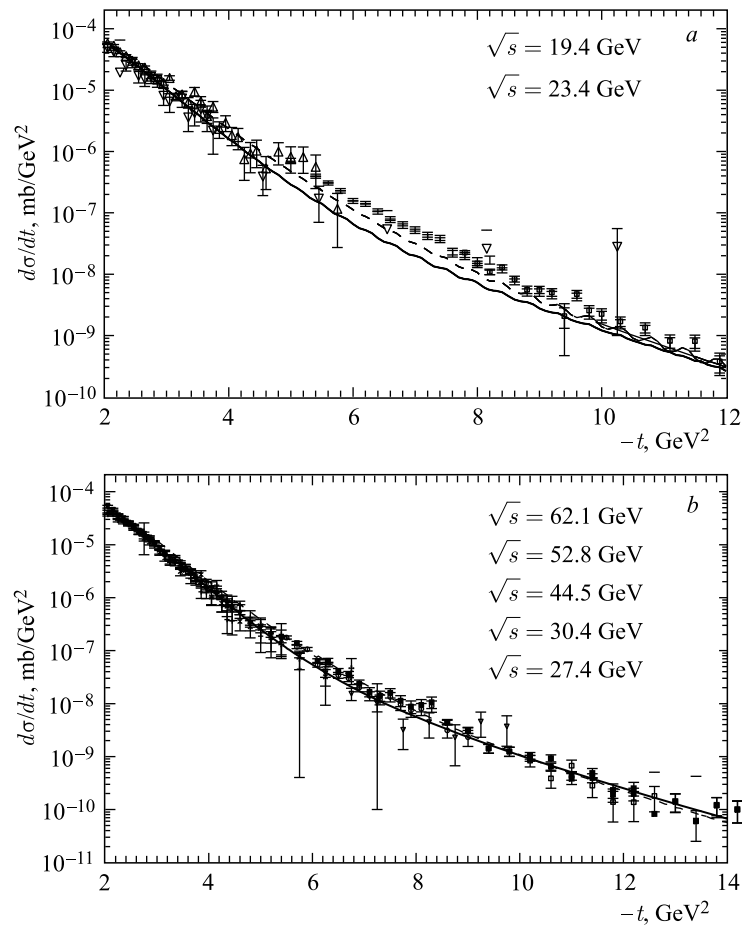


Fig. 4. Differential cross sections of the proton–proton elastic scattering at large momentum transfer (solid line — the calculations at $\sqrt{s} = 19.4$ GeV, dashed line — the calculations at $\sqrt{s} = 52.8$ GeV). a) Experimental data at $\sqrt{s} = 19.4$ and 23.4 GeV; b) experimental data at $\sqrt{s} = 27.4$ – 62.1 GeV

of the energy-independent spin-flip amplitude, Eq. (13), allow one to describe the differential cross sections at large momentum transfer. The experimental data on the differential cross section of the elastic proton–proton scattering at large momentum transfer show the small energy dependence (see Fig. 4). The HEGS model calculations reproduce such a small energy dependence of the differential cross sections at large t (see Fig. 4).

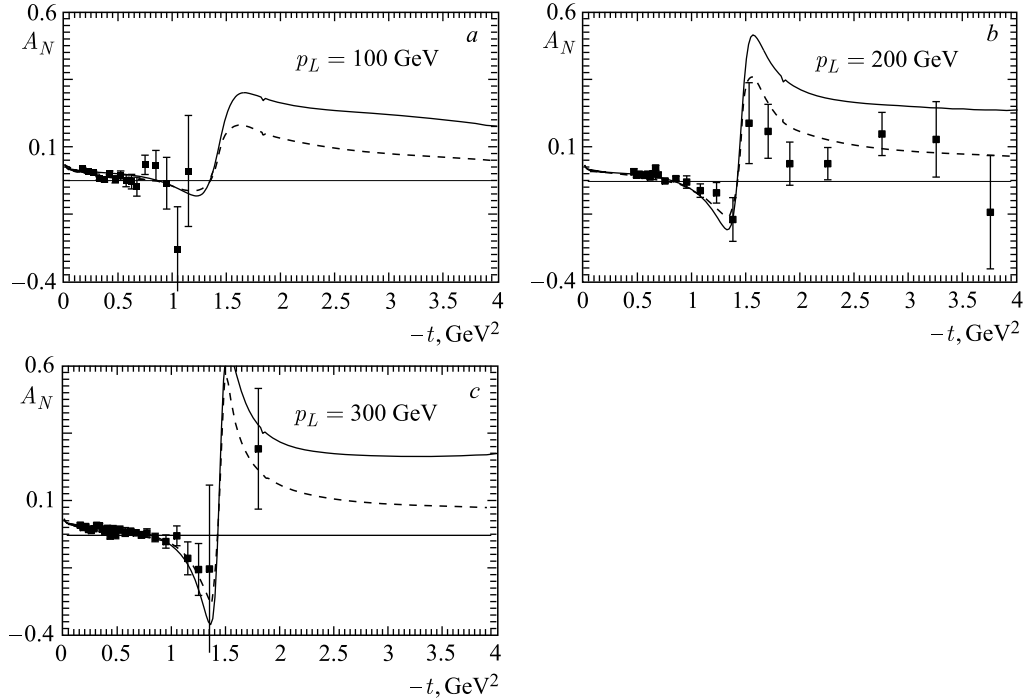


Fig. 5. The spin-correlation parameter $A_N(s, t)$ for the elastic proton–proton scattering at $p_L = 100$ GeV, $p_L = 200$ GeV, and $p_L = 300$ GeV. (Solid line — model calculations with the spin-flip amplitude, Eq. (13); dashed line — the model calculations with the spin-flip amplitude, Eq. (14); points — the experimental data [42–44])

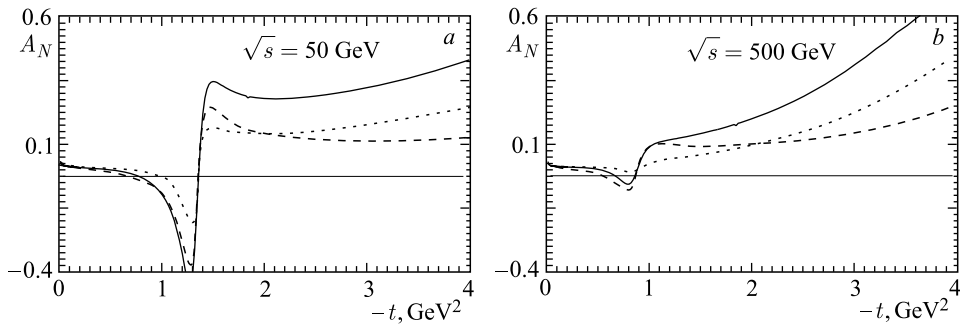


Fig. 6. The same as in Fig. 5 (additional dotted line — the calculation with the spin-flip amplitude, Eq. (13), with the standard factor $\sqrt{|t|}$ at $\sqrt{s} = 50$ GeV (a) and at $\sqrt{s} = 500$ GeV (b))

Now let us calculate in the framework of the HEGS model the spin-correlation parameter $A_N(s, t)$ in the region of the diffraction minimum. The comparison with the existing experimental data at higher energies, where the experimental data are available, $p_L = 100$ GeV, $p_L = 200$ GeV, $p_L = 300$ GeV, is shown in Fig. 5. In the last case, the diffraction minimum has a large dip. We can see that both amplitudes, Eqs. (13) and (14), give a similar picture and qualitatively agree with the existing experimental data. However, for a quantitative description new more precise experimental data at high energies are needed.

Our predictions for the spin-correlation parameter A_N are presented in Fig. 6 for two energies $\sqrt{s} = 50$ GeV and $\sqrt{s} = 500$ GeV and for all three examined spin-flip amplitudes. We can see that the total behavior is practically the same for all spin-flip amplitudes. The difference in the size of A_N is presented more remarkably at large momentum transfer.

CONCLUSIONS

The existing experimental data on the elastic hadron scattering at high energies and large momentum transfer show a small energy dependence of the differential cross sections. In the framework of the Donnachie–Landshoff model [45], such an effect is explained by the energy-independent odderon contribution. In our HEGS model, which describes the maximum experimental data in a wide energy region from $\sqrt{s} = 9$ GeV to $\sqrt{s} = 8$ TeV with minimum fitting parameters, the odderon has the same intercept as the standard soft pomeron. Taking into account the form of the spin-flip amplitude, proposed in the works of Galynskii–Kuraev [41], the energy independence of the differential cross sections at large momentum transfer is explained by the contribution of the energy-independent part of the spin-flip amplitude. The obtained size and momentum transfer dependence of the spin-flip amplitude allow one to describe the differential cross sections in the region of the diffraction minimum and at large momentum transfer.

We show that such a spin-flip amplitude is related to the interaction at a small radius in the hadron. It is found that such a behavior can be modeled by the spin-flip amplitude with the standard kinematical factor proportional to $\sqrt{|t|}$, but with the Gaussian form of the slope. The spin-correlation parameter $A_N(s, t)$ calculated in the framework of the model does not contradict the existing experimental data at high energies. We hope that the forward experiments at a future accelerator can give valuable information for the improvement of our theoretical understanding of the spin-dependent hadron interactions. This is especially true for future experiments at NICA with a polarized beam and target.

Acknowledgements. The authors are grateful to J.-R. Cudell and O. V. Teryaev for fruitful discussions of some questions considered in the paper.

REFERENCES

1. *O'Fallon J. R. et al.* Interactions in High p_{\perp}^2 Elastic pp Scattering // *Phys. Rev. Lett.* 1977. V. 39. P. 733.
2. *Lin A. M. T. et al.* Dependence of Spin–Spin Forces in 90° (Center-of-Mass) Elastic pp Scattering // *Phys. Lett. B.* 1978. V. 74. P. 273.
3. *Krish A. D.* Hard Collisions of Spinning Protons // *Proc. of XII Advanced Research Workshop on High-Energy Spin Physics, Dubna, Sept. 1–5, 2009.* P. 12.

4. *Crabb D. G. et al.* High Precision Measurement of A in Large p_{\perp}^2 Spin Polarized 24-GeV/ c Proton–Proton Elastic Scattering // *Phys. Rev. Lett.* 1990. V. 65. P. 3241.
5. *Barone V., Predazzi E.* High-Energy Particle Diffraction. N. Y., 2002. 410 p.
6. *Fiore R. et al.* Forward Physics at the LHC: Elastic Scattering // *Intern. J. Mod. Phys. A.* 2009. V. 24 P. 2551.
7. *Frankfurt L. et al.* Rapidity Gap Survival in the Black-Disk Regime. arXiv: [hep-ph]/ 0710.2942.
8. *Cudell J.-R., Selyugin O. V.* Saturation Regimes at LHC Energies // *Czech. J. Phys. Suppl. A.* 2004. V. 54. P. A441.
9. *Kopeliovich B. Z., Zakharov B. G.* n -Flip Component of the Pomeron // *Phys. Lett. B.* 1989. V. 226. P. 156.
10. *Goloskokov S. V., Kuleshov S. P., Selyugin O. V.* Spin Effects in High-Energy Hadron–Hadron Scattering // *Z. Phys. C.* 1991. V. 50. P. 455.
11. *Dorokhov A. E., Kochelev N. I., Zubov Yu. A.* Proton Spin within Nonperturbative QCD // *Intern. J. Mod. Phys. A.* 1993. V. 8. P. 603.
12. *Anselmino M., Forte S.* Small-Angle Polarization in High-Energy pp Scattering through Nonperturbative Chiral Symmetry Breaking // *Phys. Rev. Lett.* 1993. V. 71. P. 223.
13. *Kochelev N. I., Korchagin N.* Anomalous Quark Chromomagnetic Moment and Dynamics of Elastic Scattering. arXiv 2014. hep-ph:1312.5094.
14. *Cudell J.-R., Selyugin O. V.* How Precisely Will the Total Cross Section Be Measured at the LHC? // *Phys. Rev. Lett.* 2009. V. 102. P. 032003.
15. *Predazzi E.* Integral Representations for Scattering Amplitudes // *Ann. Phys.* 1966. V. 36. P. 228.
16. *Capella A., Contogourisand A. P., Tran Thanh Van J.* Factorization and Constraints in Regge Pole Theory // *Phys. Rev.* 1968. V. 175. P. 1892.
17. *Bystricky J., Lehar F.* Nucleon–Nucleon Elastic Scattering and Total Cross Sections // *Rev. Mod. Phys.* 1993. V. 65. P. 47.
18. *West G. B., Yennie D. R.* Coulomb Interference in High-Energy Scattering // *Phys. Rev.* 1868. V. 172. P. 1413.
19. *Selyugin O. V.* Coulomb Hadron Phase Factor and Spin Phenomena in a Wide Region of Transfer Momenta // *Phys. Rev. D.* 1999. V. 60. P. 074028.
20. *Gonen-Tannoudji G., Salin Ph., Morel A.* A Simple Formulation of High-Energy Exchange Models in Terms of Direct-Channel Amplitudes // *Nuovo Cim. A.* 1968. V. 55. P. 412.
21. SPIRES Database: <http://hepdata.cedar.ac.uk/>.
22. *Wu T. T., McCoy B.* Theory “Bags” with Scattering // *Phys. Rev. D.* 1974. V. 9. P. 3495.
23. *Schrempp B., Schrempp F.* Strong Interaction — a Tunnelling Phenomenon? // *Nucl. Phys. B.* 1980. V. 163. P. 397.
24. *Van Hove L.* The Diffraction Pattern of pp Elastic Scattering and the Composite Structure of the Proton // *Nucl. Phys. B.* 1977. V. 122. P. 525.
25. *Block M. et al.* Theoretical Implications of Fermilab Tevatron Total and Elastic Differential Cross-Section Measurements // *Phys. Rev. D.* 1990. V. 41. P. 978.
26. *Ji X. D.* Gauge-Invariant Decomposition of Nucleon Spin // *Phys. Rev. Lett.* 1997. V. 78. P. 610.
27. *Diehl M. et al.* Generalized Parton Distributions from Nucleon Form Factor Data // *Eur. Phys. J. C.* 2005. V. 39. P. 1.
28. *Selyugin O. V.* Momentum Transfer Dependence of GPDs. arXiv: hep-ph/1510.04468.
29. *Selyugin O., Teryaev O.* Generalized Parton Distributions and Description of Electromagnetic and Graviton Form Factors of Nucleon // *Phys. Rev. D.* 2009. V. 79. P. 033003.

30. *Selyugin O. V.* Models of Parton Distributions and the Description of Form Factors of Nucleon // *Phys. Rev. D.* 2014. V. 89. P. 093007.
31. *Selyugin O. V.* GPDs of the Nucleons and Elastic Scattering at High Energies // *Eur. Phys. J. C.* 2012. V. 72. P. 2073.
32. *Selyugin O. V.* Nucleon Structure and the High-Energy Interactions // *Phys. Rev. D.* 2015. V. 91. P. 113003.
33. *Cudell J.-R., Predazzi E., Selyugin O. V.* New Analytic Unitarization Schemes // *Phys. Rev. D.* 2009. V. 79. P. 034033.
34. *Selyugin O. V.* Hard and Soft Pomerons in the Elastic Nucleon Scattering // *Nucl. Phys. A.* 2013. V. 903. P. 54.
35. *Buttimore N. H. et al.* The Spin Dependence of High-Energy Proton Scattering // *Phys. Rev. D.* 1999. V. 59. P. 114010.
36. *Akchurin N., Buttimore N. H., Penzo A.* Evaluation of the Elastic pp Single Flip Helicity Amplitude at Low Momentum Transfer and High Energies // *Phys. Rev. D.* 1995. V. 51. P. 3944.
37. *Bourrely C., Soffer J.* How to Calibrate the Polarization of a High-Energy Proton Beam? A Theoretical Prospect. arXiv: hep-ph/9611234.
38. *Martin A. F., Predazzi E.* Diffractive Effects in Spin-Flip pp Amplitudes and Predictions for Relativistic Energies // *Phys. Rev. D.* 2002. V. 66. P. 034029.
39. *Selyugin O. V., Cudell J.-R., Predazzi E.* Analytic Properties of Different Unitarization Schemes // *Eur. Phys. J. ST.* 2008. V. 162. P. 37.
40. *Cudell J.-R., Predazzi E., Selyugin O. V.* Interactions at Large Distances and Spin Effects in Nucleon–Nucleon and Nucleon–Nuclei Scattering // *Part. Nucl.* 2004. V. 35, No. 7. P. 132.
41. *Galynskii M. V., Kuraev E. A.* Alternative Way to Understand the Unexpected Results of the JLab Polarization Experiments to Measure the Sachs Form Factors Ratio // *Phys. Rev. D.* 2014. V. 89. P. 054005.
42. *Fidecaro G. et al.* Measurement of the Differential Cross Section and of the Polarization Parameter in pp Elastic Scattering at 200 GeV/c // *Phys. Lett. B.* 1981. V. 105. P. 309.
43. *Berger E. L., Irving A. C., Sorensen C.* Implications of Nucleon–Nucleon Spin-Polarization Measurements // *Phys. Rev. D.* 1978. V. 17. P. 2971.
44. *Kline R. V. et al. (FNAL-061 (DAS)).* Polarization Parameters and Angular Distributions in $\pi^+ - p$ Elastic Scattering at 100 GeV/c and in pp Elastic Scattering at 100 GeV/c and 300 GeV/c // *Phys. Rev. D.* 1980. V. 22. P. 553.
45. *Donnachie A., Landshoff P. V.* Elastic Scattering at Large t // *Z. Phys. C.* 1999. V. 2. P. 55.

Received on November 3, 2015.